PS/HI/Note 96-05
27th March 1996

The CERN Laser Ion Source

J. Collier, G. Hall, H. Haseroth, H. Kugler, A. Kuttenberger,
K. Langbein, K. Masek, R. Scrivens, B. Sharkov, T.R. Sherwood,
A. Shumshurov, J. Tambini

1. Introduction

In 1986, light ions, namely O^{6+} and S^{12+}, were successfully accelerated in the CERN complex of accelerators for the first time. The success of this light ion acceleration and its subsequent physics programme encouraged the construction of a heavy ion accelerating facility, called the Lead Ion Accelerating Facility which is now fully operational [1,2,3]. The facility is shown in Figure 1. The lead ions are produced by an Electron Cyclotron Resonance (ECR) source [4,5,6]. Pb^{27+} ions are accelerated by the linac, stripped to Pb^{53+} and multiturn injected into the Proton Synchrotron Booster (PSB). From here they pass to the Proton Synchrotron (PS), are further stripped to Pb^{82+}, before being injected into the Super Proton Synchrotron (SPS).

The next big accelerator to be built at CERN will be the Large Hadron Collider (LHC) and it is foreseen that heavy ions, in addition to protons, will form a major component of the physics programme. It can be shown that the present LIAF has to be up-graded in its particle production by a factor 20-30 and the emittance decreased to satisfy LHC demands [7].

To satisfy LHC filling it is foreseen to increase the production rate of ions in the present heavy ion linac, to accumulate and cool the beam in the former Low Energy Anti-Proton Ring and to accelerate the particles in the PS and SPS before injection into the LHC.

Another option is to generate short, high current pulses in a Laser Ion Source (LIS) and to accelerate the ions in the PSB, PS and SPS before the filling of the LHC.

This paper describes recent developments with respect to this alternative solution.

2. Apparatus

Figure 2 shows the general layout of the Laser Ion Source experiment at CERN and Figure 3 shows the layout of the target region. The CO_2 laser is a Lumonics TEA-601A of the Transverse Excitation Atmospheric type, configured in an unstable confocal cavity arrangement. It generates a light pulse with an energy of 50 J at a wavelength of 10.6 μm (infrared). This pulse can be focused onto a solid target, where a plasma is formed. The laser pulse shape is shown in Figure 4(a) and its spatial profile in Figure 4(b). The lower trace of Figure 4(a) illustrates its temporal behavior in the absence of a plasma. The first 'spike' of full width half maximum duration 50 ns, contains approximately 50% of the energy. The 'tail' contains the other 50% and lasts for about 1 μs. The upper trace in Figure 4(a) illustrates the output in the presence of the plasma. A large degree of spiking is evident which is due to the fact that the plasma behaves as a mirror once formed, reflecting the incoming laser radiation and thereby reducing the power density. This problem is overcome by increasing the distance between the target and the laser, so that the transit time of light from the laser to the target and back is greater than the duration of the first spike of laser light. This is achieved by a system of mirrors giving a separation of 35 m between laser and target resulting in a 230 ns round trip time.

The chamber containing the target is connected to a variable high voltage power supply (max. 100 kV) and is isolated from the main vacuum chamber by a ceramic insulator. The laser beam enters the target chamber through a NaCl window and is focused onto the target by a parabolic copper mirror of focal length

30 cm. The plasma is formed on the target surface, and expands through a 30 mm diameter hole in the copper mirror into the expansion region which consists of a system of telescopic tubes directly connected to the target chamber. This creates a region free of external fields for the expansion of the plasma.

At the end of this expansion region the ions are separated from the electrons and accelerated by the electric field in the extraction assembly as shown in Figure 3. The ion beam, which contains a variety of charge states, then enters a Low Energy Beam Transport line (LEBT) for transverse matching to a Radio Frequency Quadrupole Accelerator (RFQ) previously used to accelerate oxygen and sulphur ions [8,9]. The LEBT also contains two magnetic beam steerers and a retractable profile harp for profile and position monitoring.

The last section of the line is an analysis section comprising a 77° magnetic spectrometer, entrance and exit slits and several Faraday cups. The magnet has a bending radius of 0.4 m and a maximum bending force of 0.3 Tm. At the exit of the spectrometer the ions are detected using a secondary electron multiplier (SEM). A combination of a microchannel plate (MCP) and phosphor screen can be used to produce an image of the beam.

The spectrometer can be used to measure the charge state distribution of the unaccelerated ions as well as that of the accelerated ion beam. It is also used to measure the energy of the beam accelerated in the RFQ.

The main chamber is evacuated using a 500 l/s turbo-molecular pump and a 500 l/s ion getter pump. The RFQ is pumped by two 1000 l/s cryogenic pumps and the spectrometer has an additional 50 l/s ion getter pump. The base pressure in the main vacuum chamber is typically 10^{-6} Torr.

The experiment is controlled by a computer system based on the LabVIEW control software using a GPIB bus to address CAMAC modules.

In principle any solid material can be used as a target in the LIS. However, for the experiments described below, only two target materials were used. These are tantalum for heavy ion investigations and aluminium for the acceleration experiments with the light ion RFQ. Tantalum is used in preference to lead as a heavy ion target, primarily to limit the damage caused to the copper mirror and the NaCl entry window by the deposition of target material. Due to the higher melting point, far less material is evaporated off a tantalum target than is the case for lead. Tantalum has the additional advantage of isotopic purity, resulting in easier interpretation of results.

3. Heavy Ion Experiments

3.1 Laser Produced Plasma

A plasma is formed when a high power laser beam is focused onto a solid surface and this surface absorbs some of the laser radiation. The temperature rises, the surface material subsequently evaporates and a plasma is formed. The primary mechanism of plasma heating is that of the Inverse Bremsstrahlung [10] process, where plasma electrons absorb energy from the incident radiation. These electrons then collide with the other particles present, thereby transferring energy from the

laser radiation to the plasma. Simultaneously, loss mechanisms, such as various radiation processes, cause a cooling of the plasma and a localised thermal equilibrium ensues. The local thermal equilibrium implies a Maxwellian character for the electron energy distribution and therefore allows the assignment of an electron temperature. The electron temperature of the heavy ion plasma encountered in our source is of the order of 200 to 300 eV. This has been determined by measurements of the x-ray spectrum emitted from the plasma assuming local thermal equilibrium [11].

The absorption of the laser radiation occurs up to a surface where the plasma has an electron density known as the critical density. On this surface the radiation has both a maximum of absorption and reflection, therefore no further optical propagation into the plasma is possible.

Multiple charge state ions are produced in the plasma by stepwise ionisation of the ions present from earlier electron-ion collisions. For the temperature quoted above, it is possible to produce charge states with ionisation potentials up to approximately 1 to 1.2 keV, considering that the electron energy distribution has a high energy tail.

The most relevant properties of the plasma and the resultant ion beam are, in our case, the distribution of charge states, the energy distribution associated with each charge state, the ion current density at the source exit and the ion beam emittance.

3.2 Charge State Distribution

The charge state distribution of the ions produced in the plasma can be measured using the magnetic spectrometer. The plasma is formed without the application of a voltage to the target chamber, so that there is no extraction field. It therefore expands the full distance to the entrance of the spectrometer through a region free of external fields. The transmission of the ions through the spectrometer is, at a given magnetic field, determined by their charge to momentum ratio. As the momentum spread of the ions is large, the correct momentum per unit charge to pass the spectrometer slits is present for a large number of charge states and a time of flight (TOF) spectrum can be recorded at the exit of the spectrometer using the SEM.

The complete charge state distribution is obtained by recording these spectra for a range of magnetic fields. The individual TOF traces are then combined by computer to produce a 3-dimensional representation of the charge state distribution. Such plots are shown in Figure 5 for a tantalum plasma, the shading indicating the level of the electron multiplier output signal. An absolute measure of the number of incident ions is not possible, as the secondary electron coefficient of the SEM varies with charge state and these coefficients are not known for highly charged heavy ions.

The spectra in Figure 5 were recorded with a drift distance of 3.12 m from target to detector. The upper most line in Figure 5(a) represents Ta^{2+}. Charge states up to Ta^{23+} were detected. The low charge states are dominant at longer drift times and the high charge states are clustered together at earlier times. Figure 5(b) shows the earlier part of the spectra with a higher resolution. The lower charge states exhibit evidence of some secondary process, causing a splitting of their lines.

Similar experiments using lead have shown a maximum charge state of 31+. Experiments with aluminium and magnesium have shown maximum charge states of 11+ and 12+ respectively. Results obtained with an intermediate mass ion (copper) yield a maximum of 16+. These maximum charge states all correspond to ionisation potentials in the 1 to 1.5 kV range.

3.3 Ion Energy Distributions

From the data shown in Figure 5, the energy spectrum for each charge state can be derived, assuming that all ions are created only during the laser pulse. The splitting of the lines for the low charge states suggests that some secondary effects are present during the plasma expansion.

Figure 6 shows the distributions of energy per unit charge for Ta^{1+}, Ta^{10+} and Ta^{20+} ions. The highest charge states, represented here by Ta^{20+}, have an energy distribution of the order of 5 keV per charge. At a source potential of 50 kV this would result in a 10% energy spread for the high charge state ions. This is undesirable and experiments to reduce this energy distribution are summarised in section 3.7.

3.4 Ion Extraction and Current Density

The plasma expands a given distance through a region free of external fields before the ions are extracted. This is to allow the plasma density to fall to a value at which the ions can be extracted with voltages below 100 kV. The extraction system used consists of a three electrode acceleration/deceleration arrangement often used in conventional ion sources (e.g. [12]). The plasma is created at a positive source potential and the ions are accelerated by a negative extraction electrode. The beam is then decelerated by the final grounded electrode of the extraction system. The negative potential of the extraction electrode is used to prevent the acceleration of secondary electrons into the source, as these electrons provide some compensation of the space charge of the accelerated beam. The negative voltage also allows the variation of the extraction voltage at a fixed source potential.

Due to the large peak extraction current (up to 100 mA for heavy ions and approaching 1 A for light ions) it is necessary to provide capacitive backing to the high voltage supplies, to ensure that the extraction voltages remain within an acceptable range of their nominal values. Series resistances to the electrodes are used to limit the current in the event of an electrode breakdown. The current to each electrode is monitored by current transformers.

Figure 7 shows the current measured in a Faraday cup placed immediately after the extraction system, for the case of tantalum ion extraction. The drift distance before extraction was set to 0.6 m, the electrode voltages were +60 kV, -10 kV and 0 V, the outlet aperture diameter was 15 mm and the extraction gap was 15 mm. The initial spike of the pulse has a duration of approximately 5 μs and a current of 50 mA. It is followed by a second current maximum. This second part however, contains only the low charge states and is therefore of minor interest. From Figure 5 it can be seen that the high charge states (Ta^{13+} to Ta^{23+}) arrive at the extraction

region first. From the velocity distribution it can be deduced that after a drift of 0.6 m these high charge states are found only in the first current peak (Figure 7). The current density at the maximum of this initial peak is 29 mA cm^{-2}. The average current density throughout the 5 μs of this peak is about 17 mA cm^{-2} Assuming an average charge state of 16+, the average extracted ion flux is 3.1×10^{10} ions/cm^2 during this time.

To ensure the extraction of all the ions in the high charge state peak, it is important to choose a sufficiently high extraction voltage to match to the ion current to the extraction system. The effect of the application of insufficient voltages can be seen in Figure 8. The currents measured in the Faraday cup (I_{FC}), the current in the high voltage line to the target chamber (I_P), the current measured on the negative electrode (I_N), the current on the ground electrode (I_G) and the sum of the currents ($I_{SUM}= I_{FC}+ I_N+ I_G$) are plotted for a range of source potentials. For high extraction voltages the current leaving the target chamber (I_P) roughly equals the current I_{FC} measured in the Faraday cup. As the voltage is reduced, an ion current is measured on the negative and ground electrodes and I_{SUM} becomes larger than I_P, due to electron emission from the electrode surfaces.

The extraction of ion beams from a laser plasma is complicated by various processes: Firstly, the ions have a large energy spread and the energy with which the ions arrive at the extraction system varies with time. Secondly, the charge state distribution of the ions arriving at the outlet aperture is also time dependent, i.e. the average charge state decreases during the pulse. Thirdly, it is not known whether a well defined plasma boundary, as known from the extraction from quiescent plasmas, is established during the short pulse. The shape of such a plasma boundary, however, determines the initial direction of the extracted ions. In other ion sources, the plasma density is adjusted to create a concave plasma meniscus to obtain an initially convergent ion beam. As the shape of the plasma boundary depends strongly on the plasma density, a modulation of the beam current is transformed into a temporal variation of the initial convergence of the beam. A change of the CSD with time has a similar effect.

Computer programs such as IGUN [12] and AXCEL [14] can be used to simulate the extraction process in the static case, provided that the plasma parameters are known. However, certain assumptions must be made, e.g. the initial ion velocity must be smaller than the electron velocity to avoid the creation of a negative plasma potential.

To study the temporal behaviour an attempt was made to simulate ion extraction using the program MAGIC [15]. This program allows the simultaneous treatment of electrons and various charge states of ions and can be used to study the temporal evolution of an expanding plasma. Figure 9 shows the obtained result for the extraction of tantalum ions using the conditions described in Figure 7 and assuming an energy distribution according to the data on Figure 6. Only two charge states, i.e. Ta^{10+} and Ta^{20+} were considered. (Note the expanded scale in r.)

One can observe the formation of a concave boundary at which all electrons are reflected (the ion beam appears darker on the plot), comparable to the boundary found in other simulation programs. A separation of the two charge states becomes visible at the entrance of the ground electrode. This is due to the assumption of initially equal ion velocities in the plasma, which results in a different rigidity of the different ions in the electric field.

At higher beam currents the plasma boundary becomes convex with the resulting in a diverging ion beam. These simulations show that the perveance of the extracted

beam should be in the region $1\text{-}2\times10^{-6}\times(z/A)^{1/2}$ [$A/V^{3/2}$] (with z = charge state and A = mass number). Therefore a source potential of 50 kV should correspond to 60 mA extracted beam current.

3.5 Charge State Distribution of the Extracted Beam

A charge state distribution analysis, similar to that described in Section 3.2, was performed on the extracted ion beam to determine if there is a significant change from the distribution found in the plasma. The result for a tantalum ion beam extracted under the conditions described above is shown in Figure 10. In this figure, the low charge states of the tantalum ion beam are present at higher magnetic fields.

The interpretation of the spectrum is more complicated than in the case without acceleration. In comparison with Figure 5, there are many additional lines in the low charge state region which last for long times. These satellite lines can be attributed to recombination [16]. Further satellite lines on the lower left of the plot are due to light ion contaminants, such as oxygen and carbon. The high charge states towards the bottom left of the picture are however free of additional lines. It can also be seen that these high charge states are present very early during the ion pulse and appear well before the lower charge states and extraneous ions.

3.6 Beam Emittance

The charge states of interest are only present for a few μs during the first spike of the extracted ion pulse. Thus, to measure the emittance, it is necessary to use a device which can be activated for that specific part of the beam pulse only. Due to variations from pulse to pulse and due to the low repetition rate, it is desirable to perform the measurement during a single shot.

The apparatus used is shown schematically in Figure 11. The ion beam impinges on a foil containing a square array of holes, each with a diameter of 80 μm. This foil is positioned 25 mm after the final extraction electrode. The beamlets which pass through the holes are detected after a drift of 145 mm by means of a microchannel plate (MCP) and phosphor screen assembly which turns the spatial pattern of the arriving beamlets into a light pattern on the screen. This pattern is then imaged onto the input plane of an image intensified CCD camera and recorded by computer. The MCP is activated by a 1 kV pulse of ~800 ns duration which is positioned at the point of interest during the ion current pulse. The resulting image intensity is then integrated in a vertical or horizontal direction and a phase space plot is constructed [17]. Figure 12 shows the phase space plot obtained during the 800 ns time window located at the peak of the 60 mA high charge state pulse. The emittance is 100 mm.mrad for 90% of the beam current at an extraction voltage of 50 kV.

Measurements made at two different times and thus at different currents during the first pulse give the phase space ellipses shown in Figure 13. The emittance remains constant but the shape of the ellipses is different.

3.7 Reduction of Energy Spread

As mentioned in Section 3.3, the high charge state ions in the plasma can have large energy distributions of the order 5 kV per charge. This corresponds to a 10% energy spread at 50 kV extraction voltage. Experiments to reduce this energy spread have been conducted by using a source potential which increases in time. The early part of the pulse containing the high energy ions is therefore extracted using a lower voltage than the late part containing the ions with the lower energies. The energy spread of the resulting ion beam can thus be reduced.

Figure 14 gives an example of what can be achieved. The MCP/phosphor screen assembly was positioned at the exit of the magnetic spectrometer and the exit slits were removed. This provided a means of observing the image produced by two adjacent charge states of the accelerated tantalum ion beam. The energy spread can be estimated from the width of the produced images. Figure 14(a) shows the images of Ta^{18+} and Ta^{19+} for a beam extracted at a constant source potential of 63 kV. Figure 14(b) shows the same two charge states when the source potential is increased from 54 kV to 64 kV over a period of 8 μs coincident with the initial peak of the ion pulse . Figure 14(c) is a plot of the integrated intensities of shown in Figure 14(a) and (b). A narrowing of the image is evident and corresponds to a reduction in energy spread from about 10% to approximately 3%.

4. Light Ion Experiments

4.1 Light Ion Extraction and RFQ Matching

The preceding discussions concerned the production of highly charged heavy ions and some of the properties of the heavy ion beams generated. The next step in the development of the source was to accelerate an ion beam in an RFQ structure (Figure 2), since RFQs form the first bunching and accelerating structure of modern linacs. At CERN such an accelerator, which was formerly used for the acceleration of sulphur and oxygen ions [8,9], was available.

As this RFQ was designed for the acceleration of light ions only, the element chosen as a target material was Aluminium. The RFQ input energy of 5.6 keV/u corresponds to 15 kV extraction voltage for Al^{10+}.

If light elements are used, the plasma density produced with the Laser Ion Source is very high. Therefore the length of the expansion chamber was set to the maximum possible with the present apparatus, to keep the total extraction current low. Two sets of extraction electrodes were used with either 10 or 15 mm apertures.

Figure 15 shows the ion current measured at 10 μs in a Faraday cup at a distance of 100 mm after the extraction system. The initial spike with a current >120 mA lasts for about 3 μs in this case. At the required low source potential, this large current leads to a mismatch of the extraction system (c.f. section 3.4) and also results in a very high space charge of the beam. However, although 90% of the total current was lost, the best results were obtained with these extraction conditions.

Following extraction, the correct input conditions for the RFQ are provided using the Low Energy Beam Transport Line (LEBT). The first element in this line is an electrostatic Einzel lens. It has an aperture diameter of 100 mm and was located at a distance of 650 mm after the ground electrode of the extraction system. The amount of current entering this lens was approximately 15 mA and a large amount of the total extraction current was lost on the relatively long drift. The second lens in the line which provides the final focusing to the RFQ is a pulsed magnetic solenoid lens with an inner diameter of 44 mm.

To optimise the lens parameters, the MCP was placed at the input plane of the RFQ and the beam profile was measured during the part of the ion pulse containing the required charge states. The gating facility allowed the determination of the correct settings of the two lenses for the relevant part of the current pulse. Apertures were used to fix the correct input angle for the RFQ.

4.2 RFQ Acceleration

Once the optimum conditions were found the ion current at the input plane of the RFQ was measured using an aperture restricted Faraday cup. Approximately 5 mA was present during the first spike of duration 4 μs. This part of the current pulse was known to contain the highest charge states. Al^{10+} which was the largest component of the beam was chosen as the nominal ion to be accelerated by the RFQ.

The RFQ was installed in the position of the MCP and after a further optimisation of the parameters, the output current of the RFQ was measured using a Faraday cup at the RFQ exit (Figure 16). Approximately 3 mA was accelerated by the RFQ. Considering that the RFQ has a theoretical transmission of 65% under these space charge and energy spread conditions [18,19], this a good result. The charge state distribution of the output beam was found to contain Al^{9+} and Al^{10+} in approximately equal proportion. A full description of the light ion RFQ experiments can be found in [20].

5. Discussion and Future Developments

The results above have demonstrated a number of positive aspects of the use of a laser produced plasma as an ion source. There has been a clear demonstration that substantial quantities of high charge state heavy ions ($6x10^{10}$ ions in 5μs) can be produced by the Laser Ion Source at CERN. The extraction of these ions from the plasma was accomplished and the emittance of the resultant beam could be measured. The results achieved for tantalum, and also of lead ions from the LIS, encourages further development towards a source satisfying LHC requirements for luminosity. Although the intrinsic energy spread of the high charge state heavy ions produced by the source is relatively large, a method of reducing this to a more acceptable level has been found.

Furthermore, a high current, high charge state light ion beam has been produced and successfully accelerated in a radio frequency quadrupole structure, an important milestone for the project.

The next stage in the development of the Laser Ion Source experiment at CERN will be to demonstrate that also a heavy ion beam produced by a LIS can be accelerated in an RFQ and possibly be injected into the Lead Ion Accelerating Facility. A dedicated RFQ structure is currently under construction for this purpose [21]. Additionally, work is progressing on the design of a laser capable of producing three times the output energy of the existing system with a repetition rate of 1 Hz [22].

6. References

[1] H. Haseroth, *The CERN heavy ion accelerating facility*, 1995 Particle Accelerator Conference, Dallas 1995.

[2] D. J. Warner, *The heavy ion linac for the CERN lead ion facility*, LINAC 94, Tsukuba, 1994.

[3] N. Angert, M.P. Bourgarel, E. Brouzet, R. Cappi, D. Dekkers, J. Evans, G. Gelato, H. Haseroth, C.E. Hill, G. Hutter, J. Knott, H. Kugler, A. Lombardi, H. Lustig, E. Malwitz, F. Nitsch, G. Parisi, A. Pisent, U. Raich, U. Ratzinger, L. Riccati, A. Schempp, K. Schindl, H. Schönauer, P. Têtu, H.H. Umstätter, M. van Rooij, D. Warner (Editor), M. Weiss, *CERN heavy-ion facility design report*, CERN 93-1. CERN, Geneva. 1993.

[4] M. P. Bougarel, C.E. Hill, H. Haseroth, K. Langbein, E. Tanke, *Performance of the ECR Ion Source of CERN's heavy ion injector,* Proc. 12th Int. Workshop on ECR Ion Sources, Riken, April 1995.

[5] C. E. Hill, K. Langbein, *Pulsed ECR Source in Afterglow Operation at CERN*, Proc. ICIS'95, Vancouver, 1995.

[6] K. Langbein, *Experimental Investigation of the Afterglow of the Pulsed ECR Discharge*, Proc. ICIS'95. Vancouver. 1995.

[7] LHC Study Group, *The Large Hadron Collider, Conceptual Design*, Editors P.Lefevre and T. Pettersson, CERN AC 95-05(LHC), 1995.

[8] B. H. Wolf, K. Leible, P. Spädtke, N. Angert, J. Klabunde, B. Langenbeck, R.A. Gough, J. Staples, R. Caylor, D. Howard, R. MacGill, J. Tanabe, *Performance of the oxygen injector for the CERN Linac 1*, GSI-86-2. GSI. Darmstadt. 1986.

[9] J. Staples et al., *Initial Operation of the LBL heavy ion RFQ*, Conf. on High-Energy Accelerator. Batavia, IL, USA, August 1983.

[10] K. Mima, H.A. Baladis, A. Nishiguchi, H. Takabe, C. Yamanaka. *Laser Plasma Theory and Simulation*, Harwood Academic Publishers, Switzerland, 1995.

[11] A. Kuttenberger, Diploma Thesis, Erlangen, Germany.

[12] J.R. Coupland, T.S. Green, D.P. Hammard, A.C. Riviere, Rev. Sci. Instrum. **44-9**, 1258, 1973

[13] R. Becker, W.B. Herrmannsfeldt, *A program for the simulation of positive ion extraction including magnetic fields.* Proceedings of the 4th Int. Conf. on Ion Sources. pp2756-22758, Bensheim, Germany, 1991.

[14] E.F. Jaeger, I.C. Whitson, *Numerical simulation for axially symmetric beamlets in the Ducpigatron Ion Source*, ORNL/TM-4990. Oak Ridge, TN. 1975.

[15] B. Goplen, L. Ludeking, D Smithe, G. Warren, *MAGIC Users Manual. Mission Research Corporation,* MRC/WDC-R-326. Newington, Virginia, 1994.

[16] G. Hall, S. Kondrashev, H. Kugler, R. Scrivens, B. Sharkov, R. Sherwood, J. Tambini, *Recombination processes in a highly charged ion beam extracted from a Laser Ion Source,* PS/HI Note 95-19(Tech), CERN, 1995.

[17] J. Collier, B. Goddard, G. Hall, A. Shumshurov, J. Tambini, *Emittance measurements on the CERN Laser Ion Source*, CERN PS/HI Note 95-07(Tech). 1995.

[18] A. Lombardi, *Preliminary Study of the performance of the LBL RFQ with a beam from the laser ion source*, CERN PS/HI Note 93-05. 1993.

[19] J. Staples, Private Communications. E-mail to H. Haseroth, 22.9.92

[20] A. Kuttenberger, *Entwicklung einer Laser-Ionenquelle zur Erzeugung hochgeladener Ionen für das CERN LHC Projekt*, PhD Thesis, Erlangen, Germany, 1995.

[21] A. Lombardi, *Possible RFQ designs for a lead ion beam generated by a Laser Ion Source,* PS/HI Note 94-03, CERN 1993.

[22] *Investigation of highly-charged heavy ion generation. CO_2 laser ion source design. Final report of Annex to Memorandum of Understanding between the European Organisation for Nuclear research (CERN) and the Institute for Laser Physics (ILP)*, Troitsk, Moscow region, 1995

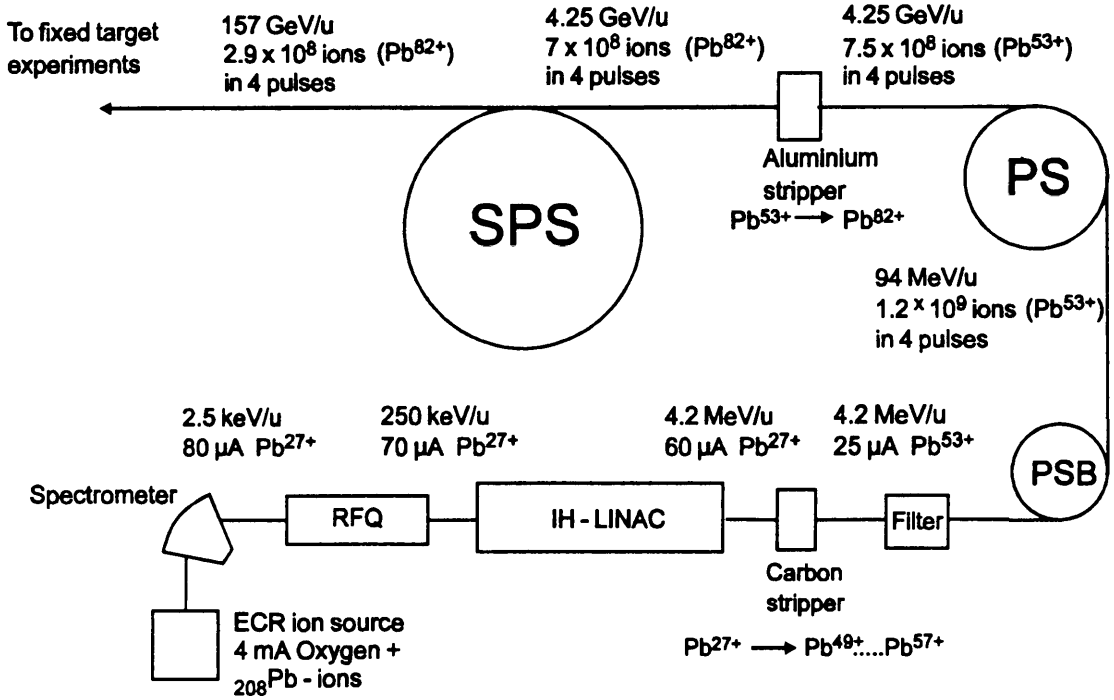

Figure 1. CERN LIAF.

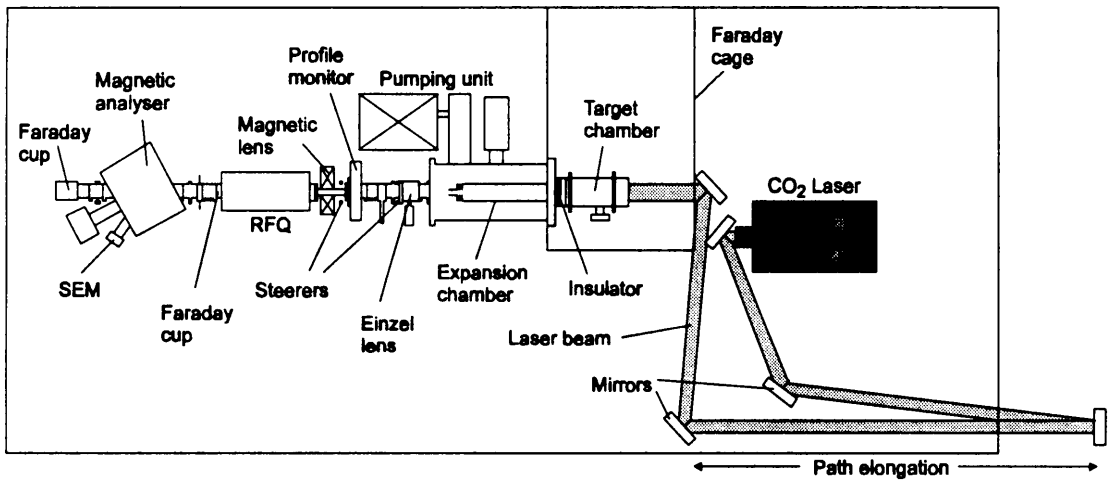

Figure 2.Plan of experimental apparatus.

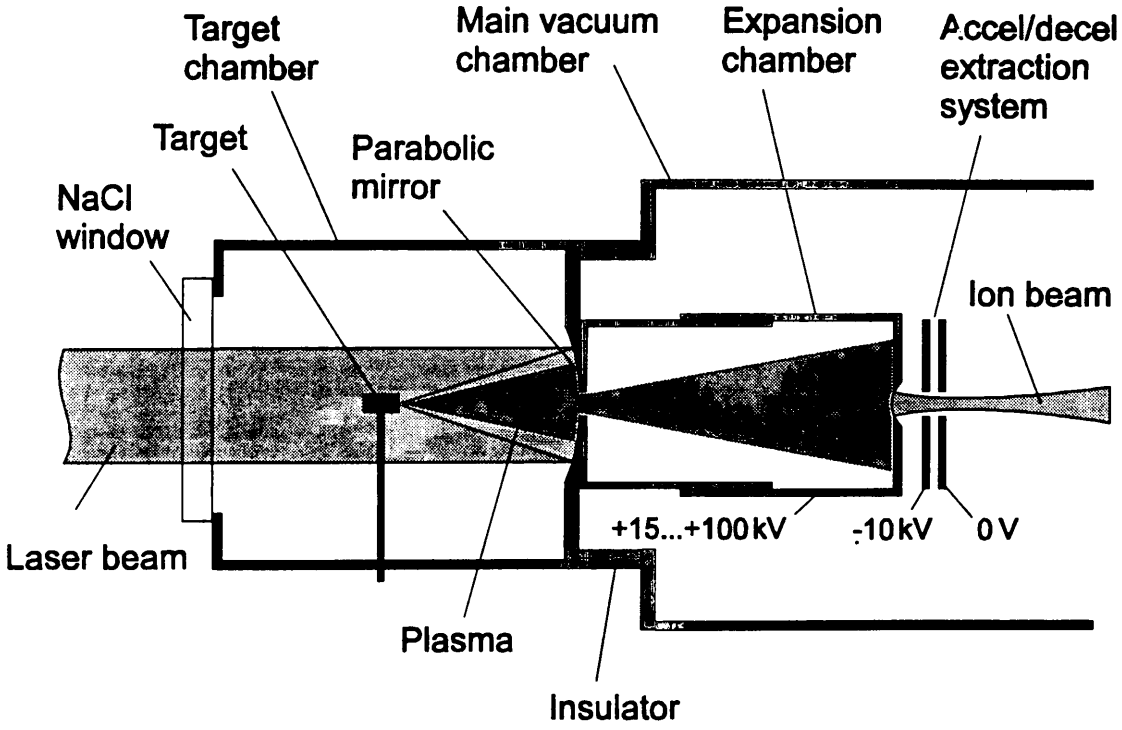

Figure 3. Scheme of the CERN Laser Ion Source.

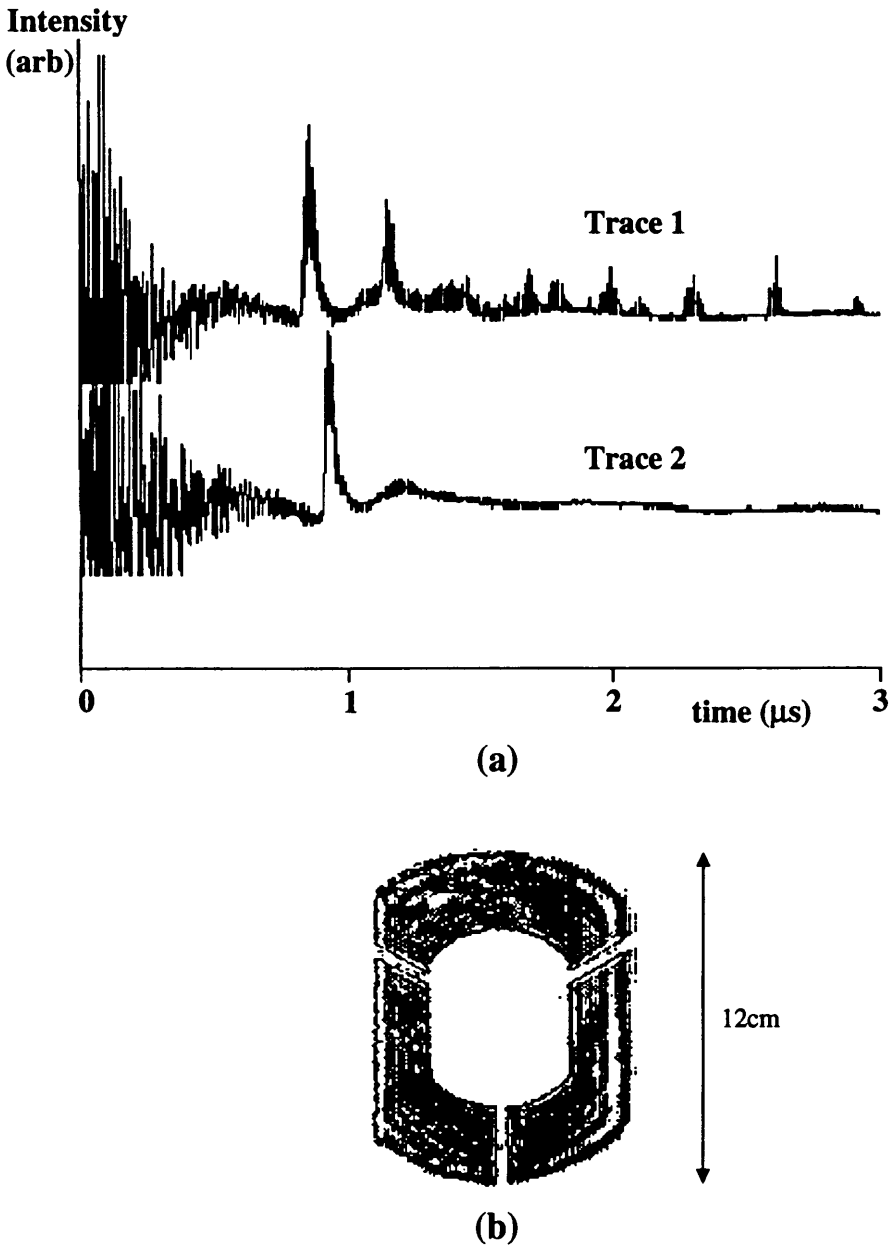

Figure 4. (a) Temporal profile of the laser beam. Trace 1- with plasma., Trace 2- Without plasma. (b) Transverse profile of the laser beam measured at the laser output window.

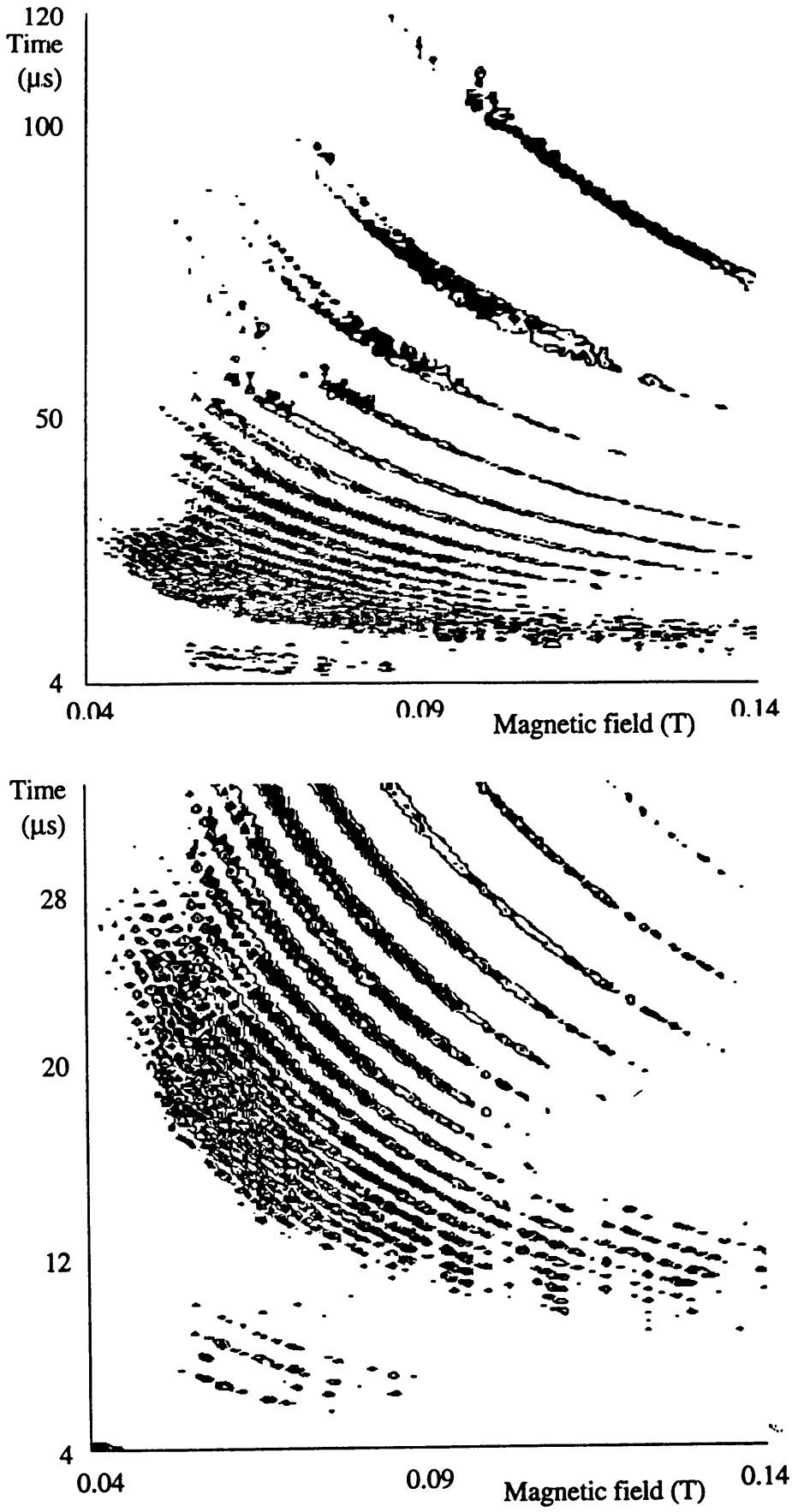

Figure 5. Charge state distribution of Ta plasma measured after the spectrometer. (a) Full 4-120 μs time scale. (b) 4-32 μs time scale.

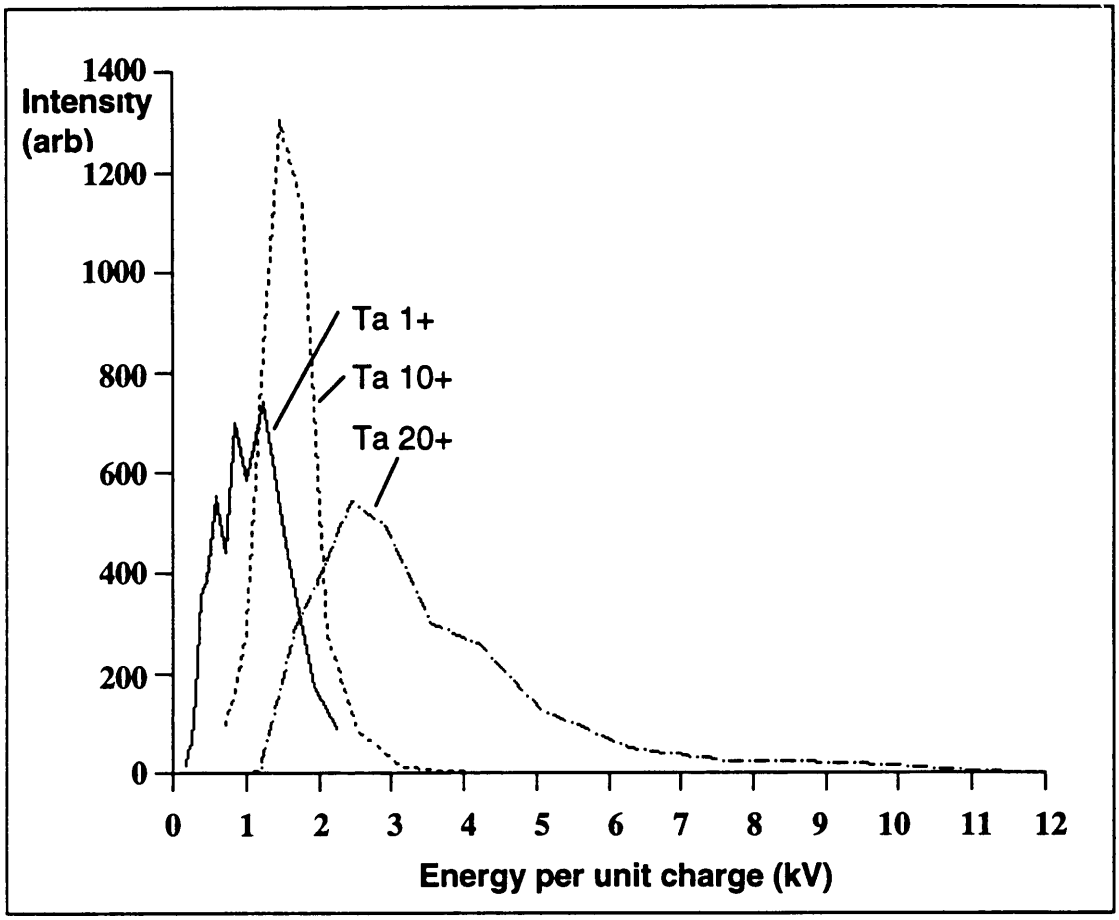

Figure 6. Energy per unit charge distribution for Ta^{1+}, Ta^{10+} and Ta^{20+}.

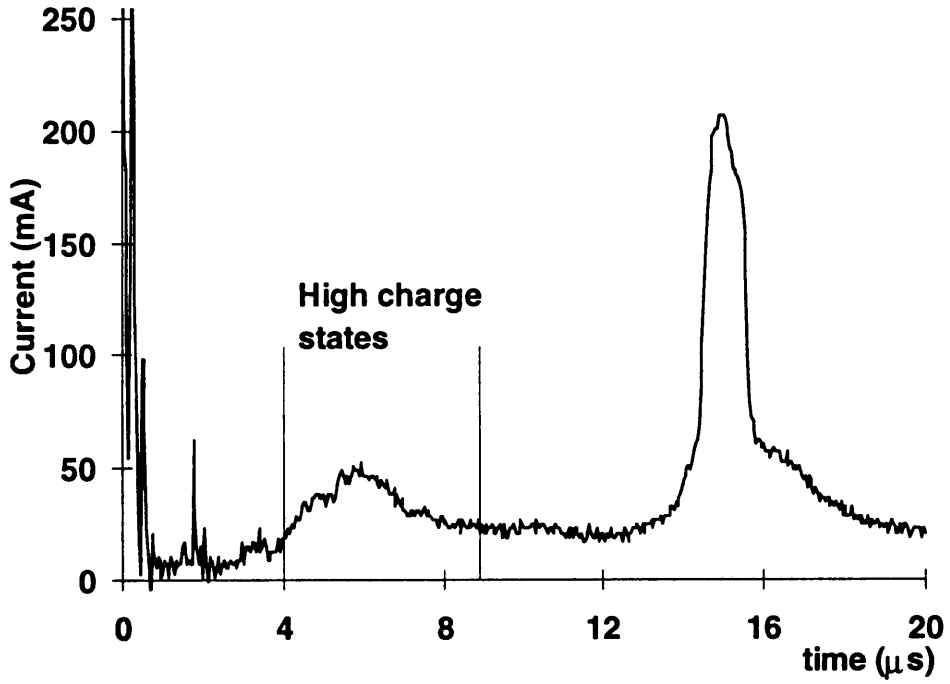

Figure 7. Tantalum ion beam current measured in a Faraday cup.

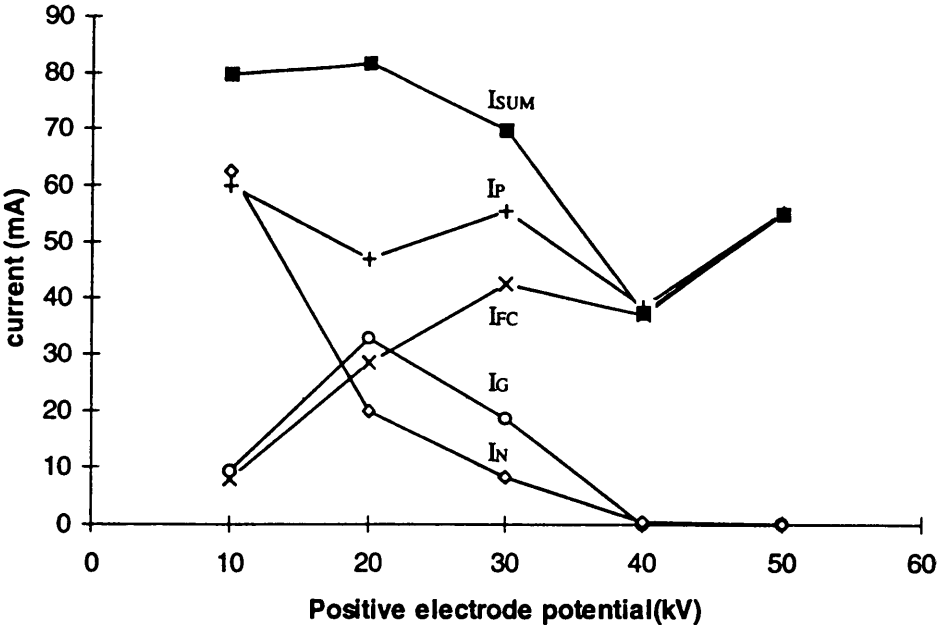

Figure 8. Ion beam currents measured to the extraction electrodes and in a Faraday cup. I_N=Negative electrode, I_G=Ground electrode, I_{FC}=Faraday cup current, I_P=Positive electrode, $I_{SUM}=I_{FC}+I_N+I_G$.

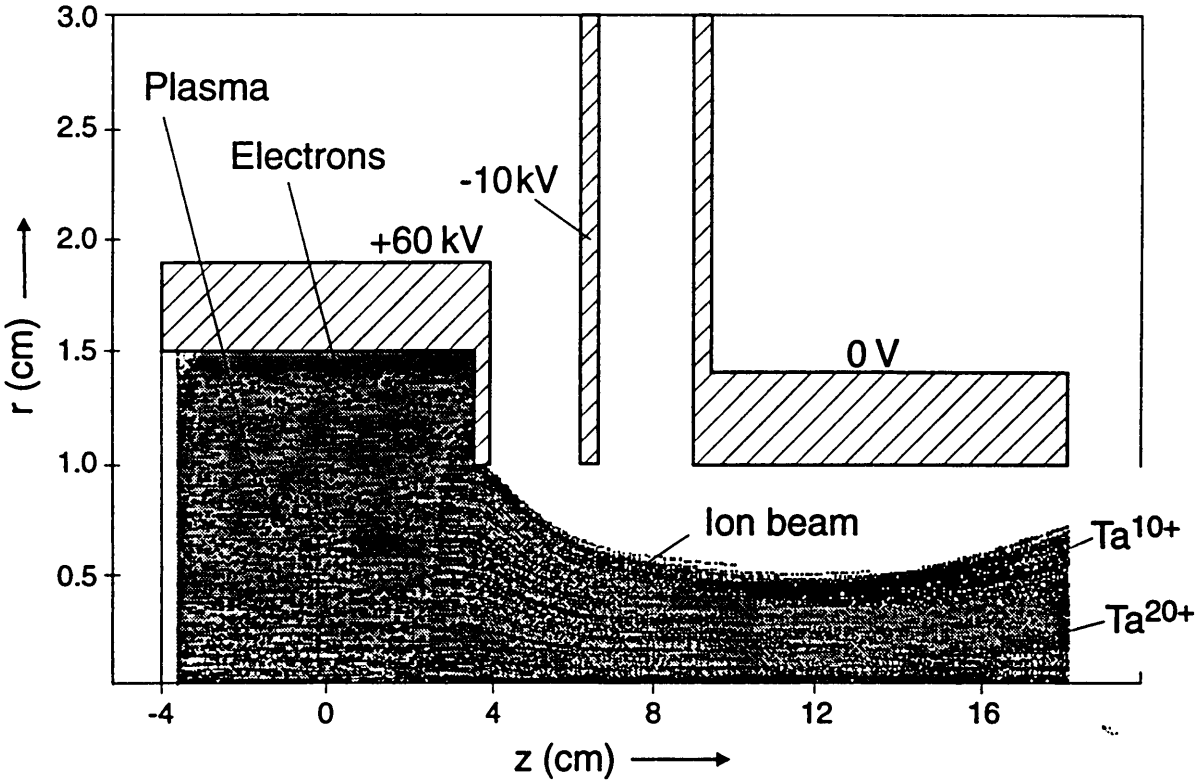

Figure 9. Simulation of ion extraction using the program MAGIC. Only 3 particle types are are considered: electrons, Ta^{10+} and Ta^{20+}.

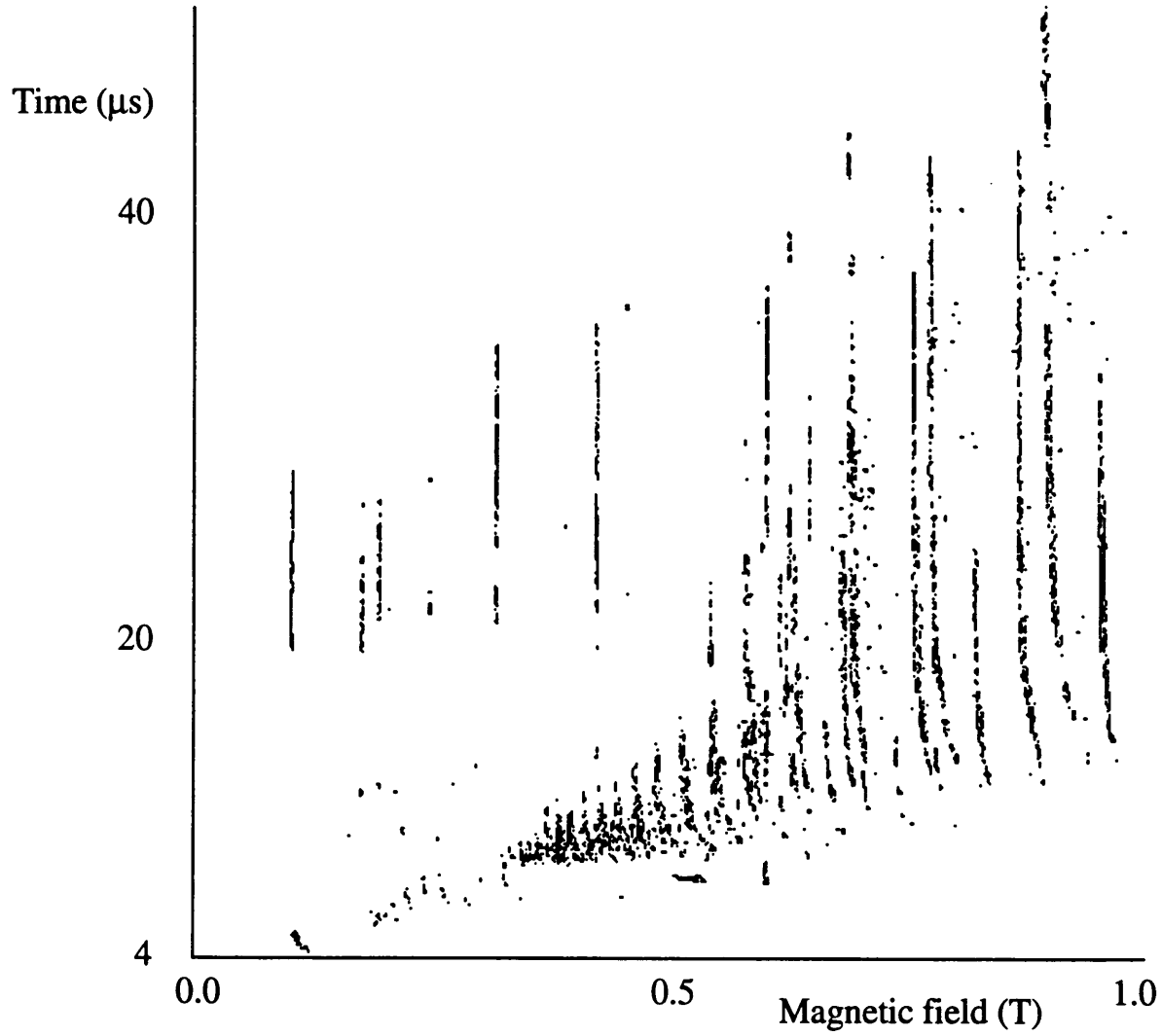

Figure 10. Charge distribution of extracted Ta beam measured after the spectrometer.

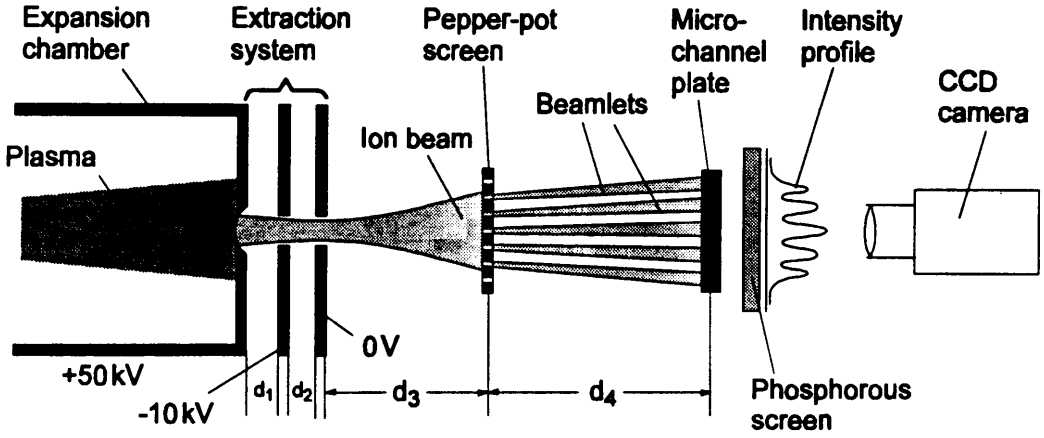

Figure 11. Emittance measurement using a pepper-pot screen. d_1=15 mm, d_2=15 mm, d_3=25 mm, d_4=145 mm, aperture radius of extraction system = 7.5 mm.

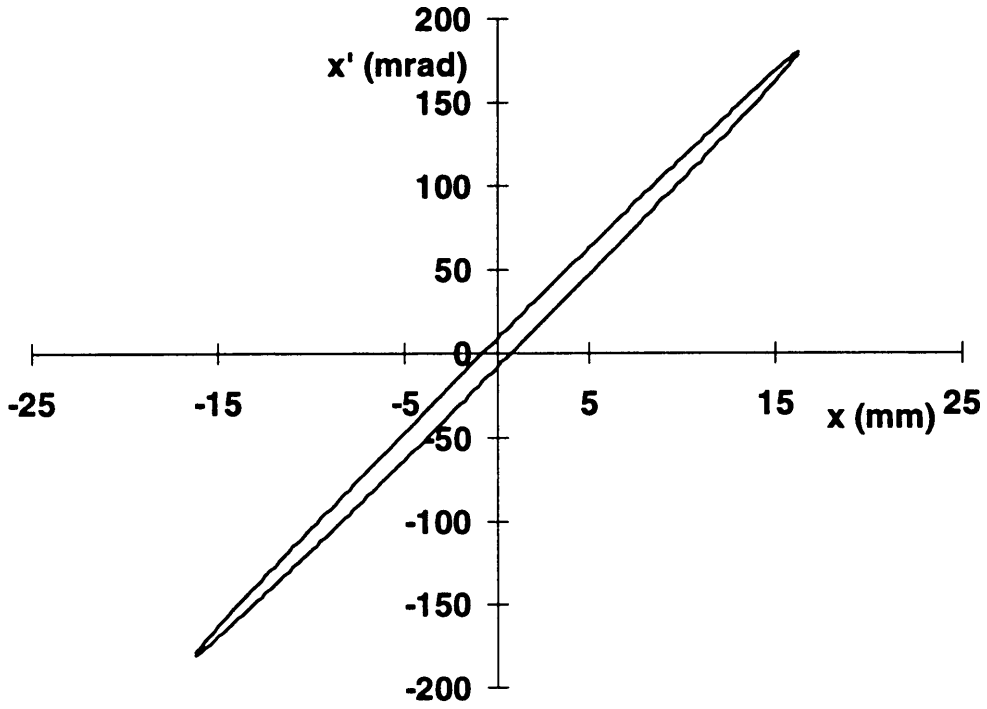

Figure 12. Transverse phase space ellipse for a 60 mA Ta ion beam after 66 kV extraction.

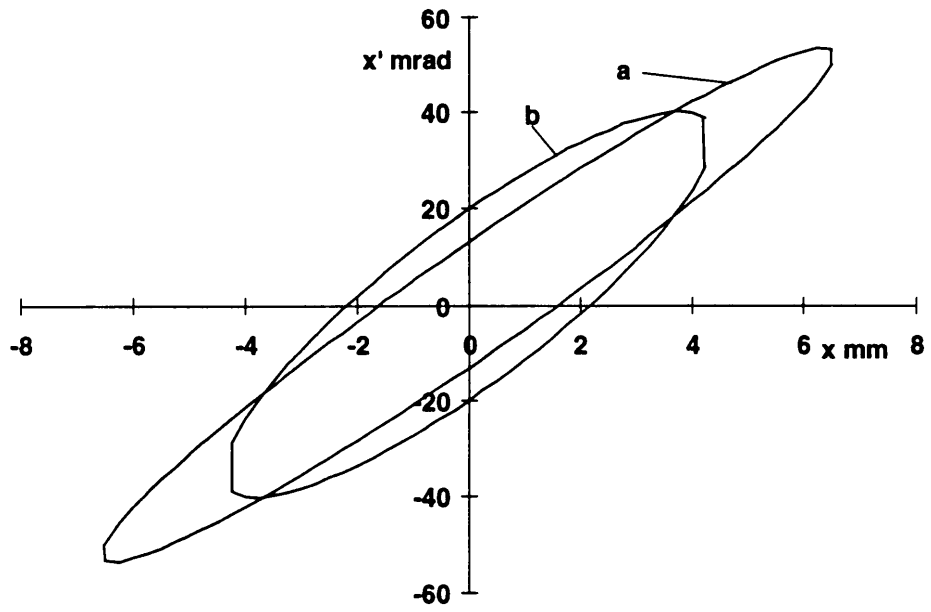

Figure 13. Transverse phase space ellipse for a Ta ion beam after 66 kV extraction. a) Measured during the current peak (45 mA). b) Measured during the current tail (10 mA).

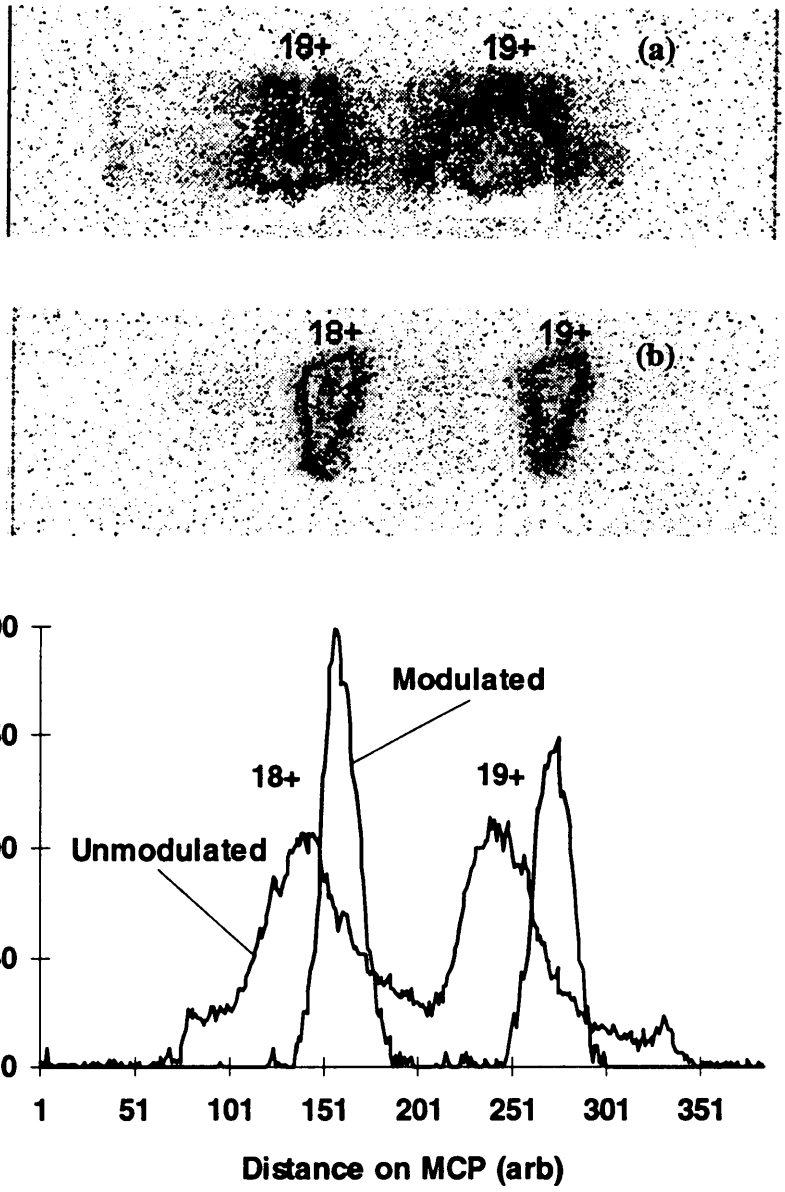

Figure 14. a) and b) CCD camera images after spectrometer for a) unmodulated and b) modulated extraction voltages. c) Vertical integration of the images.

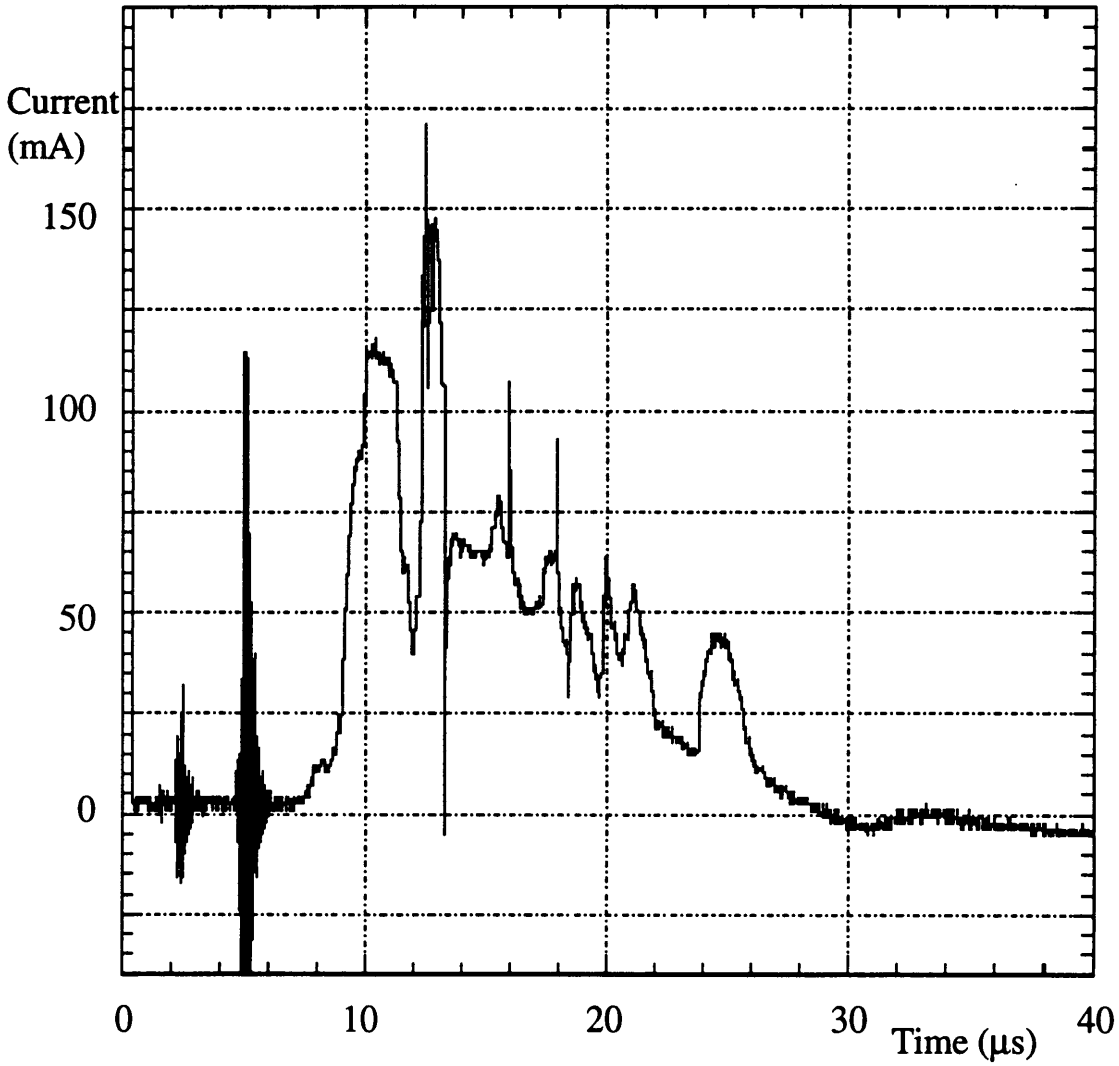

Figure 15. Aluminium ion beam current measured in a Faraday cup placed 100 mm after extraction.

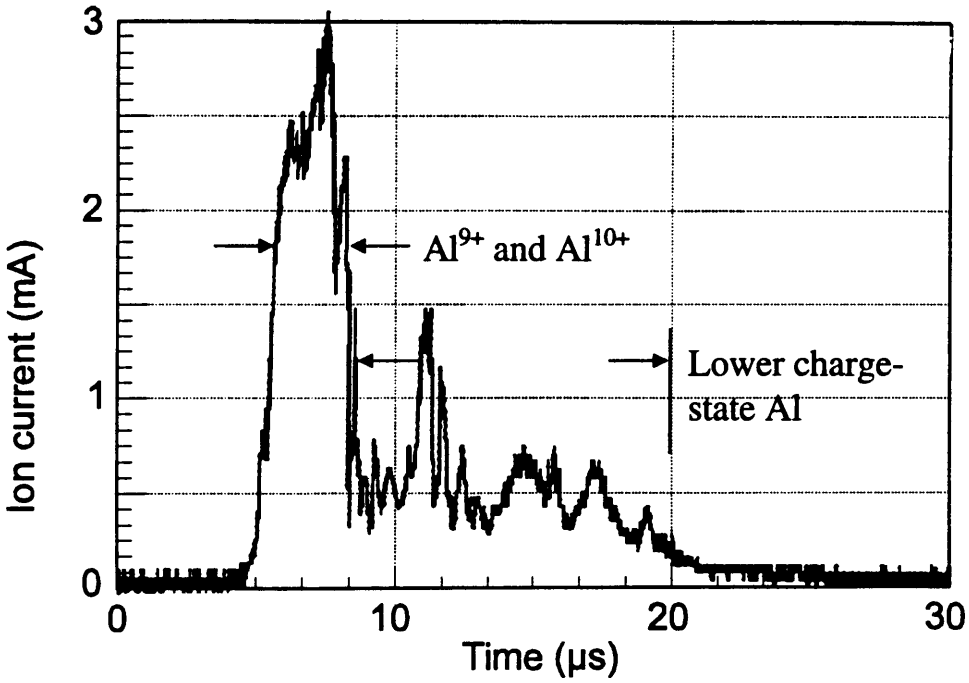

Figure 16. Aluminium ion current measured in a Faraday cup after the RFQ.